Modification in the efficiency of dye-sensitized solar cells (DSSCs) by H ions implantation on TiO_2 photoanode

M. Irfan [a], M. I. Khan [a,*], Ikram-ul-Haq [a], I. Ahmad [b], W. Shahid [a], I. Ahmad [c], Ihab M. Moussa [d], S. Mumtaz [e]

[a]*Department of Physics, The University of Lahore, 53700, Pakistan*
[b] *Department of Physics and Astronomy, Texas Tech University, Lubbock, TX 79409, USA*
[c]*Department of Applied Physics, The Hong Kong Polytechnic University, Hong Kong*
[d]*Department of Botany and Microbiology, College of Science, King Saud University, P.O. Box 2455, Riyadh, 11451, Saudi Arabia*
[e]*Electrical and Biological Physics, Kwangwoon University, Seoul, 01897, South Korea*

The sol-gel approach was utilized to synthesize the pure TiO_2 films. Hydrogen ions are irradiated on these synthesized films with a flow rate of $2x10^{13}$, $2x10^{14}$ and $2x10^{15}$ ions-cm^{-2}, and the beams are accelerated at 700 KeV. The XRD analysis confirmed the tetragonal structure of TiO_2. The high grain size is observed at $2x10^{14}$ ions/cm^2. UV-visible spectroscopy showed that films are highly transparent to visible light and hydrogen ions produces a red shift in the absorbance peak. The low value of E_g is observed at $2x10^{14}$ ions/cm^2. The calculated value of conduction band edges gave suitable information of the behavior of free charge carriers in the solar cells. PL analysis showed that the recombination rate reduced, which will enhance the dye-sensitized solar cells' efficiency. DSSCs have been prepared with these films. The EIS results indicate the resistance in the transportation of charges across the interfaces reduces. Via current voltage J-V analysis, open circuit voltage V_{oc}, short circuit current density J_{sc} and fill factor FF were improved with the H-irradiation process at $2x10^{14}$ ions/cm^2 fluence rate, resulting in maximum photoconversion efficiency of 4.05%.

(Received June 24, 2024; Accepted January 21, 2025)

Keywords: Ions implantation, Proton, TiO_2, Dye sensitized solar cells

1. Introduction

To full fill the energy demand of the overgrowing population was the motive behind the development of solar cells. The pollution-free energy production can be obtained through solar cells, and the endless energy source (sun) is behind its high acceptance [1]. Traditional Si-junction solar cells are expensive because of their complex production processes and high purity raw material requirements. The dye-sensitized solar cells are fascinating and practical replacements to junction-based (silicon) solar cells due to their accessible fabrication method and low-cost raw materials [2]. The fundamental idea behind DSSC was first presented by Michael Gratzel and Brian O' Regan. They put idea of covering the semiconducting material with dye for obtaining maximum light harvesting ability [3]. The efficiency of DSSCs depends upon the characteristics of the semiconducting material of photoanode. TiO_2 is considered the most promising material among the other semiconducting materials currently employed to prepare photoanodes in DSSCs. Titanium dioxide is a transparent material for visible light, having a wide band gap suited for UV radiations for photocatalytic activity. It has excellent stability, is readily available, cheap, and non-toxic. Because the energy band gap of TiO_2 is high and not appropriate for the visible light photons to inject electrons into its CB via dye and the excited electron, due to insufficient energy,

* Corresponding author: muhammad.iftikhar@phys.uol.edu.pk
https://doi.org/10.15251/DJNB.2025.201.89

will again jump to lower energy states [4, 5]. The TiO_2 photovoltaic activity for visible electromagnetic region can be increased by incorporating some suitable elements into its crystal structure [6]. Thus, the use of TiO_2 in pure form is restricted; the high rate of electron-hole pair recombination lowers the dye-sensitized solar cell's efficiency. Its band gap tuning and doping with different elements can overcome these limitations. A dye-sensitized solar cell has been reported with a photoconversion efficiency of 6.05% when the nanaoparticles of TiO_2 are treated with hydrogen. In that study, TiO_2 nanoparticles were deposited on an FTO glass substrate [7]. Hydrogen, because of smaller sized atoms, can easily penetrate TiO_2 crystal lattice, thus modifying the optoelectronic properties of resulted material and enhancing its light-harvesting property [8, 9]. Compared to other doping materials used for tuning TiO_2, hydrogen is highly pure, minimizing the possibility of impurities from reducing agents and solvents integrating with the TiO_2 [10].

In the present study TiO_2 nanostructured films are implanted with H ions at the fluence rates of $2x10^{13}$, $2x10^{14}$ and $2x10^{15}$ ions-cm^{-2} because the main advantages of ion implantation include precise control over the implanted dose, area, and depth profile.

2. Characterizations

The material's structural properties can be investigated through the X-ray powder diffraction (XRD) technique using a Malvern Panalytical equipment with Cu-K_α radiation (1.5418 Å) in the range of 20^0 to 80^0. TiO_2 absorbance spectra of both pure and H-irradiated is obtained via UV-Vis spectrophotometer (U-0080D). The data obtained from the photoluminescence spectroscopy give deep insight about the electron-hole recombination process. The Keithley 2400 (Abet Technologies) data recorder equipment was utilized to measure the photocurrent-voltage (J-V) characteristic curves at an irradiation level of 100 mWcm^{-2} (AM 1.5 spectrum).

3. DSSC fabrication

The photoanode of the dye-sensitized solar cells is prepared by the deposition of TiO_2 on the FTO glass substrate. These films are irradiated with H ions at flow rates of $2x10^{13}$, $2x10^{14}$ and $2x10^{15}$ ions-cm^{-2}. The films are soaked in N719 dye for 20 hours for better absorption. The Pt counter electrode is fabricated on an FTO substrate. The counter electrode and the photo anodes are sealed with parafilm to ensure no electrolyte leakage is possible. Through a tiny hole bored into the counter electrode, the iodide/tri-iodide electrolyte is injected between the sealed electrodes.

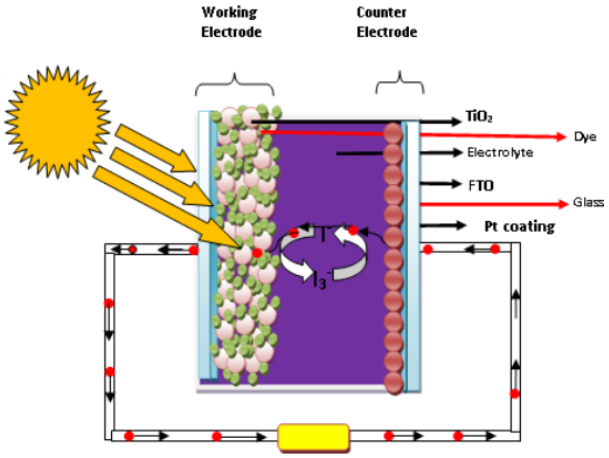

Fig. 1. Diagrammatic illustration of a dye-sensitized solar cell .

After filling the electrolyte, the hole is sealed. Four dye-sensitized solar cells are fabricated in this way, in which one is pure, and three are prepared with H-irradiated TiO_2 thin films. Figure 1 presents an illustration of these developed cells. The efficiency of the developed cells was assessed using the J-V measuring method. Surface profilometer is utilized for the measurement of the film thickness.

4. Results and discussion

4.1. XRD analysis

The diffractogram exhibits the highest intensity peak (101) for both pure and H-irradiated TiO_2 at 2θ values of 25.32°, 25.28°, 25.25° and 25.30° at fluence rates of $2x10^{13}$, $2x10^{14}$ and $2x10^{15}$ ions/cm^2 respectively. All the peaks are identical anatase having tetragonal symmetry verified by the JCPDS card No. 21-1272. In the diffractogram of all the plots of pure and H-irradiated samples, the peak (101) has the highest intensity, indicating that all samples are anatase. The anatase peaks are shifting toward a lower angle, indicating that the interlayer distance between the adjacent layers is increasing due to H presence in the TiO_2 crystal structure. The H is small ionic radii element that fills the interstitial spaces of TiO_2, changing the lattice structure. Thus, the crystallinity of the resulting material after the irradiation process decreases, which is observed by the decrease in the peak intensity. As d and θ have inverse relation so, peak shifting towards a lower angle is observed [11]. The lattice strain at high fluence rate 2 $x10^{15}$ ions/cm^2 of H ion on TiO_2 shifts peak again towards higher angle side.

The average crystallite size is determined through the use of the Debye-Scherer equation, which is indicated by relation 1.

$$D = \frac{K\lambda}{\beta cos\theta} \tag{1}$$

Each of the three lattice parameters (a, b, c) are calculated by using the following relation

$$\frac{1}{d^2} = \frac{h^2+k^2}{a^2} + \frac{l^2}{c^2} \tag{2}$$

In above relation the Miller indices are h, k and l, d is the separation between the adjacent atomic layers. The volume of the tetragonal crystal symmetry is calculated using relation given below

$$V = a^2 \text{x c} \tag{3}$$

The quantities determined by the above relations are summarized in Table 1

The peak intensity was found to shorten after the irradiation process by hydrogen ions irradiated at 700 KeV, and peaks get broader is an indication that the crystallinity of the sample reduces. The peak broadening can be determined from the X-ray diffractogram illustrated in Figure 2 with the help of FWHM. The reduction of the peak intensity is also verified by the crystallite size, which for the pure sample is 21.75 nm. For the H-irradiated films at a flow rate of 2 $x10^{13}$ ions/cm^2, 2 $x10^{14}$ ions/cm^2, and 2 $x10^{15}$ ions/cm^2 the average crystallite sizes are 14.83 nm, 20.10 nm and 19.29 nm, respectively. So, a clear reduction trend in the crystallite size is observed with the H-irradiation process. This decrease in the peak intensity and peak broadening can be associated with the asymmetry in the crystal lattice due to the H atoms in TiO_2. This H has small ionic radii (0.53 Å) compared to Ti (0.67 Å). The TiO_2 crystal lattice becomes somewhat amorphous as a result of this tiny hydrogen filling the interstitial spaces. As a result, crystallite size decreases due to inhibition of crystal formation. As demonstrated by Figure 2, the crystallite size increases once more when the flow rate approaches 2 x 10^{15} ions-cm^{-2}, probably as a result of the development of the rutile phase.

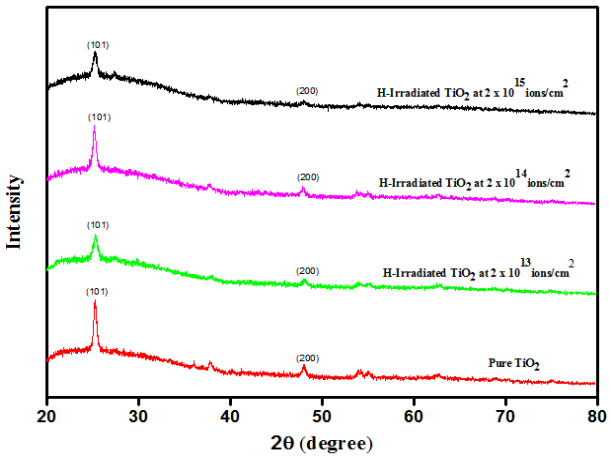

Fig. 2. Diffractogram of titania in various fluence rates, both pure and irradiated with H.

Table 1. XRD investigations of TiO_2 films at various fluency rates that are both pure and H-irradiated.

Sample	2θ	FWHM	Interplanar spacing d(Å)	Crystallite size D (nm)	a=b (Å)	c (Å)	V $(Å)^3$
Pure TiO_2	25.32	0.3914	3.517	21.75	3.788	9.468	135.86
H irradiated-TiO_2 at $2x10^{13}$	25.28	0.5738	3.523	14.83	3.784	9.653	138.21
H irradiated-TiO_2 at $2x10^{14}$	25.25	0.4233	3.527	20.10	3.801	9.460	136.67
H irradiated-TiO_2 at $2x10^{15}$	25.30	0.4413	3.520	19.29	3.787	9.543	136.85

The volume of the pure TiO_2 crystal lattice is 135.86 $(Å)^3$. In contrast, this volume increases upon H-irradiation to138.21 $(Å)^3$, 136.67 $(Å)^3$ and 136.85 $(Å)^3$ at fluence rates of 2 x 10^{13}, 2 x 10^{14} and 2 x 10^{15} ions/cm^2 respectively. The reason for this volume rise is the inclusion of H ions in TiO_2 crystal lattice because this H fills the interstitial spaces, resulting in an expansion of the volume. The volume decreases again when the fluence rate increases from 2 x 10^{14} ions/cm^2 to 2 x 10^{15} ions/cm^2 because the high concentration of H, the lattice get contracted due to high strain value as an excess of H may get trapped inside the grain boundaries.

4.2. UV visible spectroscopy

UV visible spectroscopy helps in measuring various optical parameters like band gap energy, absorbance, band edges position, refractive index etc. The absorbance of the electromagnetic radiation in the pristine and H-irradiated samples at flow rates of $2x10^{13}$, $2x10^{14}$ and $2x10^{15}$ ions/cm^2 are calculated in the wavelength range of 200 nm to 500 nm illustrated in Figure 3. The relationship provided below is used to measure the band gaps values [12]

$$(\alpha h\nu)^n = A(h\nu - E_g) \tag{4}$$

where α is the absorption coefficient, h is Planck's constant, and v is the vibrational frequency, band gap Eg, A representing proportional constant. n=1/2 for an indirect allowed transition and n=2 for a direct allowed transition [13]. The Tauc illustration in Figure 3 can be used for estimating Eg values by extra plotting the curves obtained in the graph plotted between $(\alpha h\nu)^2$ vs hν. The point where the extra plotted line touching the x-axis is the energy band gap value Eg .

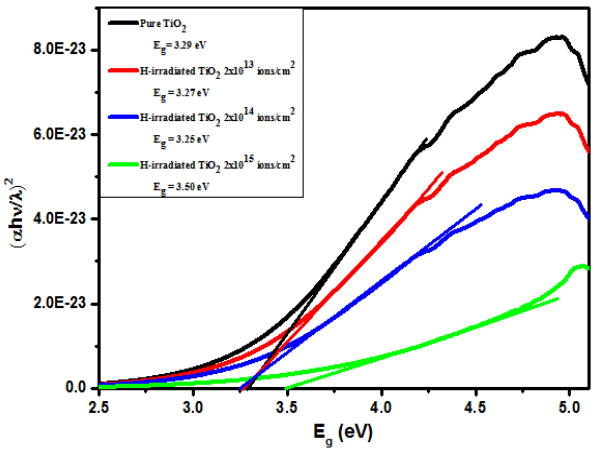

Fig. 3. Tauc plot for different fluence rates of pure and H-irradiated titania.

For the pure TiO_2, the band gap energy is 3.29 eV, but when irradiated with H ions, this band gap energy changes to 3.27 eV, 3.25 eV and 3.50 eV at a fluency rate of $2x10^{13}$ ions/cm^2, $2x10^{14}$ ions/cm^2 and $2x10^{15}$ ions/cm^2 correspondingly. The band gap value has decreased after H-irradiation may be due to the slight atomic relaxation which is obtained when interstitial H forms weak bonds with neighboring oxygen [14]. Due to smaller ionic radii of hydrogen (0.53Å) can quickly diffuse into titania crystal lattice and covers the crystal's interstitial spaces, especially in the inorganic compounds.

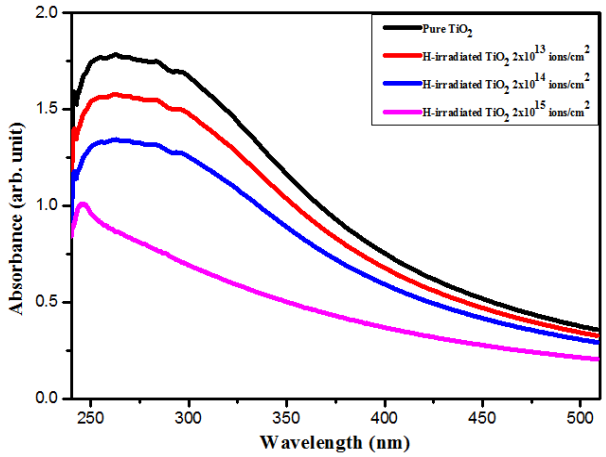

Fig. 4. Pure and H-irradiated titania's absorption spectra at different fluence rates.

The equilibrium of the crystal changes when small or big size impurity enters the host material generating the crystal defects [15]. Therefore, being small, the H ions in TiO_2 generates defects, and especially hydroxyl groups are created [16-18]. These species are the electron donor, the localized Ti–O(H)–Ti species [14, 19]. Thus, intermediate energy levels are created within the band gap of TiO_2. These defects in the energy band gap of TiO_2 provide a level for the accommodation of electrons excited from dye to TiO_2. The defects created due to the incorporation of impurity atoms into the host crystal are categorized as deep or shallow-level defects [20]. The shallow-level defects are close to the conduction band, whereas the deep-level defects are away from the band edges, sometimes in the middle of the band. The species Ti–O(H)–Ti generated due to the hydrogen will donate electrons to the shallow traps, which are present close to the conduction band edge's bottom [21]. These trapped electrons leap into the CB when thin films

come into contact with electromagnetic radiation [19]. The crystal size of TiO_2 does not significantly increases due to H insertion, but the band gap reduces due to the creation of shallow defects near the conduction band edge [22, 23]. At the fluence rate of $2x10^{15}$ ions/cm^2, the concentration of H in TiO_2 becomes high; thus, the extra amount of hydrogen will gather at the grain boundaries hindering the crystal growth and leading to the somewhat amorphous phase and disorder of the structure, leads to a rise in the Eg value [24].

The absorption spectra for the H-irradiated TiO_2 samples are better than the pure one and the red shift in the absorption was noticed for H-irradiated TiO_2 samples [7]. The absorbance is inversely related to the transmittance; when the absorbance is high means less transmittance. The sifting of the absorbance band spectrum towards the visible region is due to the generation of oxygen vacancies below the conduction band edge. The electron requires less energy to jump these energy levels. This excitation energy is available in the visible light photons; thus, light is absorbed due to these energy levels of concerning the impurities in the titania band gap. The porosity of the films also increases upon the irradiation process, which leads to a higher rate of visible photons absorption [25].

4.2.1. Band edges calculations

The relative positions of the band edges are important for explaining the electron transport mechanism from the dye's HOMO to the semiconducting material's conduction band, i.e., TiO_2. This electron shifting is essential for determining the efficiency of the DSSCs. The shifting of the bottom of the conduction band in the downward direction and the upper edge of the valance band in the upward direction is a desirable objective for obtaining high-efficiency DSSCs. For the obtaining the band edges values for the valance band edge and conduction band edges, we utilized the following relations.

$$E_{CB} = X - E_C - \frac{1}{2}E_g \tag{5}$$

where

$$X = \frac{1}{2}(E_{EA} + E_{ion})$$

The band gap energy value is E_g in the relationships above, and E_c is 4.5 eV the energy on hydrogen scale for free electron. The initial ionization energy is E_{ion} [26] and E_{EA} is referred as the electron affinity. Using that given relation, one can compute the valance band edge.

$$E_g = E_{CB} - E_{VB} \tag{6}$$

The values calculated from the utilization of the above relations are given in Table 2, and a diagram showing the band edges shifting is given in Figure 5.

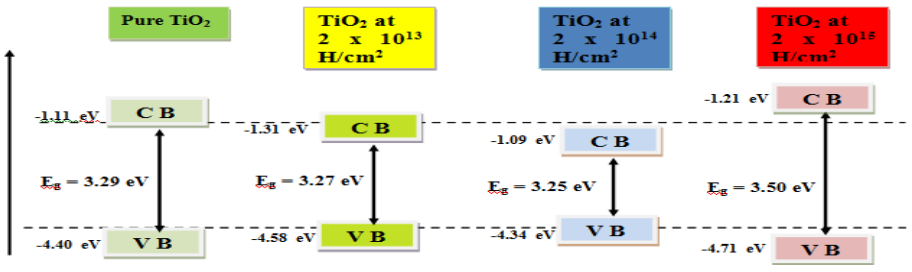

Fig. 5. Schematic for the band edges position for pure and H-irradiated TiO_2.

It is observed that band edges move close to each other after the H ions irradiation process. When the band edges are close, the injection efficiency of photogenerated electrons into the conduction band (CB) of titania increases, thus, increasing the efficiency of dye-sensitized solar cells. Hence the recombination of electron-hole pairs is restricted due to the strong driving force [27]. For the pure TiO_2 sample, the valance and the conduction band edges are far apart; thus, the injected electrons require a significant driving force to jump within TiO_2's conduction band. The photons in the visible electromagnetic spectrum do not contain this amount of energy; thus, only a fraction of the electron can jump into CB of TiO_2, which is carried by the UV photons. Therefore, due to the rapid rate at which electron-hole pairs recombination, the excited electrons quickly jump back to their parent energy level, decreasing the photoconversion efficiency of the fabricated DSSCs using TiO_2 in pure form as photoanode semiconducting material. Due to these high recombination rates, the device's temperature also increases by the photons generated by the recombination process, which adversely impacts the device's efficacy. Due to irradiation of TiO_2 with hydrogen ions, the Eg of the samples decreases. The band edges come close to each other; thus, energy in the visible light is suitable for obtaining electrons by the photoexcitation process to produce electricity. The recombination rate reduces due to the closeness of the band edges. Thus, the device efficiency is enhanced by this close shifting of the band edges. The band edges are very close when the flux of H ions on TiO_2 reaches $2x10^{14}$ cm^{-2}, and the highest efficiency is obtained because of the highest driving force, which quickly shifts the photogenerated into the CB of TiO_2, and the rate at which recombination occurs decreases. When the TiO_2 film is implanted with H ions at flow rate of $2x10^{15}$ ions/cm^2, the band edges shift away again, increasing the band gap energy of the resulting sample. This shifting is related to the disruption of TiO_2's anatase phase and the emergence of just a small portion of the rutile phase. The excess of the H ions in TiO_2 at a fluence rate of $2x10^{15}$ ions/cm^2 collected at the grain boundaries and restricted the crystal's growth. Thus, the smooth flow of photogenerated electrons is hindered, so the efficiency of DSSCs reduces.

Table 2. Band edge values for pure and H-irradiated films in the conduction and valance bands.

Sample	E_g (eV)	E_{CB} (eV)	E_{VB} (eV)
Pure TiO_2	3.29	-1.11	-4.40
H irradiated-TiO_2 at $2x10^{13}$	3.27	-1.31	-4.58
H irradiated-TiO_2 at $2x10^{14}$	3.25	-1.09	-4.34
H irradiated-TiO_2 at $2x10^{15}$	3.50	-1.21	-4.71

4.3. Photoluminescence analysis

Photoluminescence analysis is utilized to determine electron-hole pairs recombination, transfer and trapping. Photoluminescence spectroscopy is essential for describing the response of the material under which it is exposed to electromagnetic radiation. The electrons of material, after absorbing energy, are excited to higher energy levels. As a material's excited state is unstable, the electrons transition from higher to lower energy levels, they release photons of energy corresponding to the existing energy levels within the material or lies between the band gaps, if any there. These illuminations indicate the number of energy states as the possible recombination process is taking place there are responsible for these emissions. The intensity of the PL peaks describes number of photons originating from the recombination process of the electrons with their counterpart, i.e., hole. The numbers of peaks are the number of possible energy levels facilitating the recombination process. The small value of PL is the higher separation between electron holes and less recombination.

Pure TiO_2 with the highest PL intensity means the highest recombination rate of photogenerated electron-hole pairs. The peak intensity indicates a decreasing trend upon the H ions irradiation process, and the small intensity is noticed at $2x10^{14}$ ions/cm^2. The appearance of the peaks in the visible range of electromagnetic spectra because the vacancies present below the

conduction band, and these transitions are possible with low-energy photons. These are the oxygen vacancies facilitating the charge transfer process at low energy and reducing the recombination process. The emission peaks in the visible region are mostly caused by shallow or deep trap centres and excitons related to oxygen defects.

The hydrogen ions present at the interstitial spaces in the TiO_2 crystal lattice can generate deep level defect or shallow-level defects [28]. The shallow-level defects are close to the conduction band edge and are able to serve as donor states, whereas the deep-level defects are nearly at the centre of the band gap [16]. The shallow-level defects due to H-irradiation acts as the shallow donors [29]. At a flow rate of $2x10^{14}$ ions/cm^2, three PL peaks are seen in the photoluminescence spectrum at 362 nm, 372 nm, and 495 nm. The emission peak at 495 nm (blue emission) is associated with the transition from the titania valence band to localized surface states. The peak intensities are less for H-irradiated as compared to pure samples at $2x10^{14}$ ions/cm^2, is an indication that negligible recombination is observed. The shallow defects generated due to the H presence in TiO_2 increase the lifespan of the photogenerated electrons, thus decreasing the probability for the electron-hole pair recombination. The implanted ions enhance the time it takes for photogenerated electrons to recombine with their parent hole and boost the effectiveness of charge separation by adding extra energy levels to the band gap of the semiconductor [30]. So, the impurity levels act as trapping centres for improving excited photoelectron lifetime, which is desirable for obtaining high efficiency of the fabricated DSSCs. On the other hand, at a fluence rate of $2x10^{15}$ ions/cm^2, the defect levels are acting as recombination centres facilitating the recombination process resulting in a decrease in the photoconversion efficiency of the prepared dye-sensitized solar cell. Consequently, the higher concentration of H acts as a centre for electron-hole pair recombination rather than promoting charge transfer, which lowers the efficiency of dye-sensitized solar cells [31].

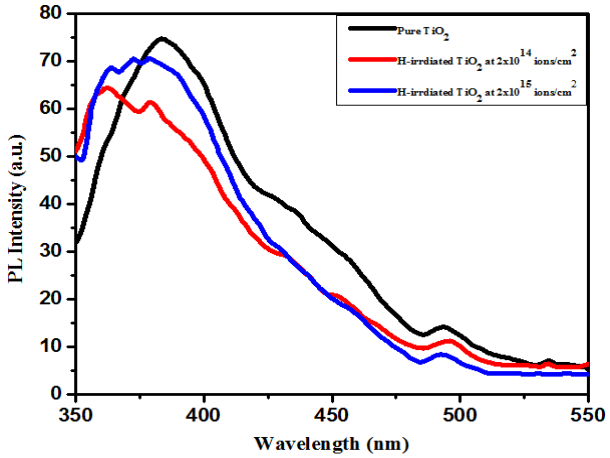

Fig. 6. Photoluminescence spectra of pure and H-irradiated samples.

4.4. Electrochemical impedance spectroscopy (EIS)

EIS is utilized to analyze the flow of charges across the various interfaces. The electrochemical impedance spectra are obtained in the form of semicircles. The impedance curve is divided into the two regions named as the transport resistance is provided the interface of TiO_2 film, dye, and electrolyte, as well as the counter electrode is the recombination resistance. The electron transport resistances at each interface were evaluated using the EIS Nyquist plot [32]. Z'' and Z', which represent the imaginary and real parts of the impedance, respectively, have been plotted on a Nyquist plot. In EIS Nyquist plots, the circular arc radius correlated with the splitting of an electron-hole pair and charge transfer resistance [33].

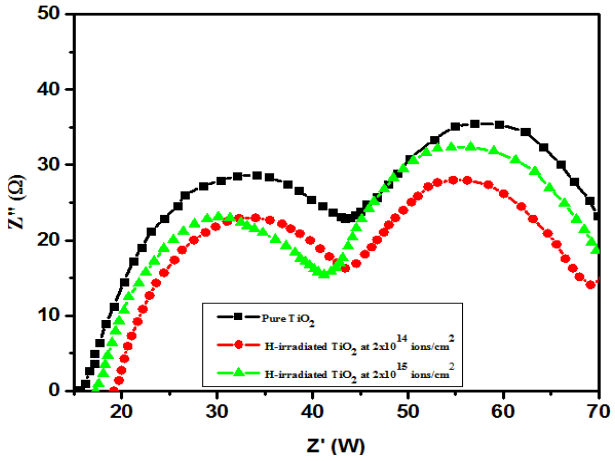

Fig. 7. EIS illustration of H-irradiated and pristine $TiO_2$0.

Figure 7 displays the corresponding EIS spectra for the pristine and H-irradiated TiO_2 photoanode at flow rates of $2x10^{13}$, $2x10^{14}$, and $2x10^{15}$ ions-cm^{-2}, respectively. It is seen clearly that the radius of a semi-circle of the plots reduces upon the H-irradiation process. This decrease in the radius of the circles indicates that the conductivity in the flow of the charge carriers decreases, and the transportation of the charges is improving. The pace at which electron-hole pairs recombine at film/dye/electrolyte interfaces reduces because the impurity generated within the band gap is a trapping centre resisting the recombination process, thereby improving charges flow. The highest flow rate is noticed at a fluency rate of $2x10^{14}$ ions/cm^2, whereas on further increasing fluence rate of $2x10^{15}$ ions/cm^2, the recombination rate increases; thus, flow rate reduces. A boost in the band gap value can be linked to an increase in the rate of electron-hole recombination, due to which the band edges move away from each other and the smooth shifting of carriers to the conduction band reduces.

4.5. J-V measurements

The dye-sensitized solar cells' photoconversion efficiency is ascertained by J-V measurements. From the J-V curve, we can evaluate open circuit voltage (Voc), Fill factor (FF) and short circuit density (Jsc). Using these values, we can calculate the efficiency of DSSC from the relation given below.

$$\eta(\%) = \frac{J_{sc} \times FF \times V_{oc}}{P_{in}} \times 100 \quad (10)$$

The incident light power is pin. Table 3 provides the values derived from the J-V curve. For pure TiO_2, the short circuit current density is 7.38 mA/cm^2. An increase in the value is observed after H-irradiation reaching 7.92 mA/cm^2. When the flow rate of H ions increases and reaches $2x10^{14}$ ions/cm^2, the value increases, getting the highest value of 8.20 mA/cm^2. Enhancing the density of short circuit current, Jsc is linked to inhibiting the recombination process. Also, the band edges come close to each other at a flow rate of $2x10^{14}$ ions/cm^2, so the transfer of charges to the conduction band becomes smooth [34]. The electron traps within the band gap that support the recombination process are removed by the presence of H ions, thus increasing the flow of charges. The higher value of the Jsc indicates that the contact between the interfaces, i.e. film/dye/electrolyte, has been improved, thus reducing the resistance by the H-irradiation process [35, 36] . The dye loading at this fluency rate is also maximum due to an enhancement in the porosity of the TiO_2 film; thus, light harvesting ability of the device increases its efficiency. Therefore, $2x10^{14}$ ions/cm^2 is the optimum value of the fluence of H ions on TiO_2. On further increasing the H ions fluency rate to 2 x 10^{15} ions/cm^2 in TiO_2, the Jsc decreases to 7.73 mA/cm^2. There are more crystallographic defects due to the increased fluency rate of lattice structure

deterioration. Higher H levels can also cause redox reactions with electrolyte ions that reduce Jsc [4].

Table 3. Solar cells parameters.

Samples	Jsc (mA/cm^2)	Voc (V)	FF	Efficiency η (%)
Pure TiO_2	7.38	0.7814	0.5530	3.19
H irradiated-TiO_2 at $2x10^{13}$	7.92	0.7866	0.6033	3.76
H irradiated-TiO_2 at $2x10^{14}$	8.20	0.7870	0.6270	4.05
H irradiated-TiO_2 at $2x10^{15}$	7.73	0.7895	0.5776	3.53

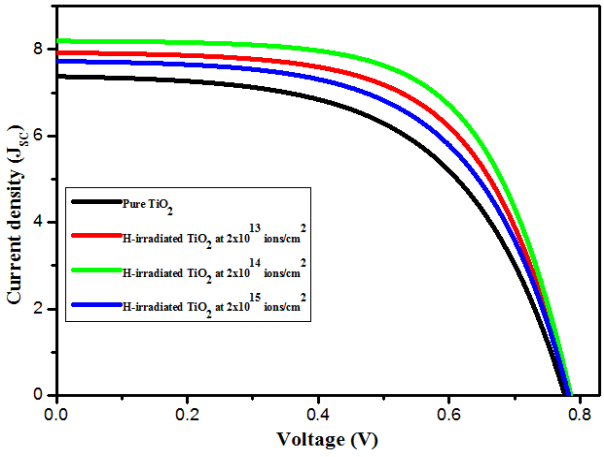

Fig. 8. J-V curve for pure and H-irradiated TiO_2 photoanode DSSCs.

A higher value of the fill factor FF indicates a lower recombination rate [37]. The highest value of FF of 0.627 is observed, which is confirmed by the PL spectra showing the lowest value at $2x10^{14}$ ions/cm^2. Because the dye adhesion gets harmed by greater H ion concentrations, aggregation causes the absorption area to decrease as well as the short-circuit current density to decrease [38]. High implanted ion concentrations increase the number of trapping sites, which causes the quantum tunneling effect, which raises recombination. More injected ion concentration levels cause implanted ions to form recombination centres, which accelerates the recombination of electrons and holes [39]. High fluence will shrink the pores, resulting in less dye adsorption and decreased device effectiveness [40].

The open circuit voltage Voc of the dye-sensitized solar cells refers to the voltage obtained across the terminals of the device, a moment electromagnetic radiation comes into proximity to the device without externally applied voltage. It is an important parameter that describes the maximum voltage obtained under illumination and directly describes the fabricated device's efficiency. The quasi-Fermi level of the photoanode and the redox potential of the electrolyte can be utilized to calculate the photovoltage (Voc). The maximum value of the open circuit voltage, 0.627 V, is obtained at $2x10^{14}$ ions/cm^2. This highest value of the open circuit voltage is associated with decreased band gap energy. By inhibiting the back electron transport, Voc and FF can be improved [41]. These changes in TiO_2 film with H ions yield the maximum efficiency of 4.05%.

5. Conclusion

The sol-gel approach has been effectively utilized to synthesize nanostructured TiO_2. Thin films of synthesized TiO_2 nano material are deposited on the substrate made of FTO glass by the dip coating method. XRD analysis confirms the anatase phase and tetragonal symmetry, and the reduction in the crystallite size is observed. The band gap energy reduces as the band edges shift close to each other, and the absorption band spectrum shows a redshift via hydrogen insertion. PL intensity decreases with the H-irradiation process and offers the lowest intensity of PL peak at $2x10^{14}$ ions/cm^2 fluency, thus the lowest rate at which electron-hole pairs recombine. The EIS analysis depicts an improved flow rate in the presence of H in TiO_2. J-V characteristics show enhanced short circuit current density, open circuit voltage and fill factor at $2x10^{14}$ ions/cm^2 fluency rate, and maximum efficiency of 4.05 % is obtained.

Funding

Researchers supporting project number (RSPD2025R741), King Saud University.

Acknowledgements

The authors would like to thank the Researchers Supporting Project number (RSPD2025R741), King Saud University, Riyadh, Saudi Arabia.

References

[1] Supriyanto, A., et al., Journal of Physics: Conference Series. 2019. IOP Publishing; https://doi.org/10.1088/1742-6596/1170/1/012048

[2] Chahid, S., D.M. de los Santos, R. Alcántara, Proceedings of the 3rd International Conference on Smart City Applications. 2018; https://doi.org/10.1145/3286606.3286854

[3] Nazeeruddin, M.K., E. Baranoff, M. Grätzel, Solar energy, 2011. 85(6): p. 1172-1178; https://doi.org/10.1016/j.solener.2011.01.018

[4] Zhou, L., et al., Chemical Physics, 2016. 475: p. 1-8; https://doi.org/10.1016/j.chemphys.2016.05.018

[5] Wang, Z.-S., et al., Journal of Physical Chemistry C, 2008. 112(43): p. 17011-17017; https://doi.org/10.1021/jp806927b

[6] Paola, A.D., et al., International Journal of Photoenergy, 2001. 3(4): p. 171-176; https://doi.org/10.1155/S1110662X01000216

[7] Javed, H.M.A., et al., International Journal of Hydrogen Energy, 2021. 46(27): p. 14311-14321; https://doi.org/10.1016/j.ijhydene.2021.01.184

[8] Xiong, K., J. Robertson, S. Clark, Journal of Applied Physics, 2007. 102(8): p. 083710; https://doi.org/10.1063/1.2798910

[9] Ramakrishnan, V.M., et al., International Journal of Hydrogen Energy, 2020. 45(31): p. 15441-15452; https://doi.org/10.1016/j.ijhydene.2020.04.021

[10] Pesci, F.M., et al., Journal of Physical Chemistry C, 2013. 117(48): p. 25837-25844;

https://doi.org/10.1021/jp4099914
[11] Subramanian, A., J.-S. Bow, H.-W. Wang, Thin Solid Films, 2012. 520(23): p. 7011-7017; https://doi.org/10.1016/j.tsf.2012.07.055
[12] Khan, M., et al., Ceramics International, 2020. 46(16): p. 24844-24849; https://doi.org/10.1016/j.ceramint.2020.06.268
[13] Kharoubi, A., et al., European Physical Journal Applied Physics, 2015. 72(3): p. 30301; https://doi.org/10.1051/epjap/2015150282
[14] Robertson, J., P. Peacock, Thin Solid Films, 2003. 445(2): p. 155-160; https://doi.org/10.1016/j.tsf.2003.08.013
[15] Peter, Y., M. Cardona, Fundamentals of semiconductors: physics and materials properties2010: Springer Science & Business Media.
[16] Rahimi, N., R. Pax, E.M. Gray, Progress in Solid State Chemistry, 2019. 55: p. 1-19; https://doi.org/10.1016/j.progsolidstchem.2019.04.003
[17] Xiao, P., et al., Sensors and Actuators B: Chemical, 2008. 134(2): p. 367-372; https://doi.org/10.1016/j.snb.2008.05.005
[18] Nowotny, J., Journal of Physical Chemistry C, 2011. 115(37): p. 18316-18326; https://doi.org/10.1021/jp204072z
[19] Panayotov, D.A., J.T. Yates Jr, Chemical Physics Letters, 2007. 436(1-3): p. 204-208; https://doi.org/10.1016/j.cplett.2007.01.039
[20] McCluskey, M., E. Haller, CRC Press. 2012; https://doi.org/10.1201/b11819
[21] Peacock, P., J. Robertson, Applied Physics Letters, 2003. 83(10): p. 2025-2027; https://doi.org/10.1063/1.1609245
[22] Filippatos, P.-P., et al., Scientific Reports, 2021. 11(1): p. 5700; https://doi.org/10.1038/s41598-021-81979-x
[23] Ataei, S.S., M.R. Mohammadizadeh, N. Seriani, Journal of Physical Chemistry C, 2016. 120(16): p. 8421-8427; https://doi.org/10.1021/acs.jpcc.6b00019
[24] Roy, S., A. Bhuiyan, Sensors and Transducers, 2015. 195(12): p. 18.
[25] Cao, F., et al., Journal of Physical Chemistry, 1995. 99(31): p. 11974-11980; https://doi.org/10.1021/j100031a027
[26] Handbook, C., Handbook of Chemistry and Physics (web edition). 2004.
[27] Wei, L., et al., RSC advances, 2015. 5(86): p. 70512-70521; https://doi.org/10.1039/C5RA15815J
[28] Wu, Q., et al., Nano Energy, 2016. 24: p. 63-71; https://doi.org/10.1016/j.nanoen.2016.04.004
[29] Herklotz, F., E. Lavrov, J. Weber, Physical Review B, 2011. 83(23): p. 235202; https://doi.org/10.1103/PhysRevB.83.235202
[30] Smirnova, N., et al., Nanoscale Research Letters, 2017. 12(1): p. 1-8; https://doi.org/10.1186/s11671-017-2002-3
[31] Li, Y., et al., Journal of hazardous materials, 2012. 227: p. 25-33; https://doi.org/10.1016/j.jhazmat.2012.04.071
[32] Sakthivel, T., et al., Materials Research Express, 2017. 4(12): p. 126310; https://doi.org/10.1088/2053-1591/aa9e36

[33] Yang, Y., et al., Journal of Photochemistry and Photobiology A: Chemistry, 2004. 163(3): p. 517-522; https://doi.org/10.1016/j.jphotochem.2004.02.008

[34] Hachiya, A., et al., Journal of Physical Chemistry C, 2012. 116(32): p. 16951-16956; https://doi.org/10.1021/jp307185d

[35] Huang, F., et al., Journal of Materials Chemistry, 2012. 22(33): p. 17128-17132; https://doi.org/10.1039/c2jm32409a

[36] Wang, H., et al., Optical Materials, 2019. 89: p. 375-381; https://doi.org/10.1016/j.optmat.2019.01.059

[37] Kaur, N., et al., RSC advances, 2019. 9(35): p. 20375-20384; https://doi.org/10.1039/C9RA02657F

[38] Sahu, K., M. Dhonde, V.V.S. Murty, International Journal of Energy Research, 2021. 45(4): p. 5423-5432; https://doi.org/10.1002/er.6169

[39] Shen, Q., D. Arae, T. Toyoda, Journal of Photochemistry and Photobiology A: Chemistry, 2004. 164(1-3): p. 75-80; https://doi.org/10.1016/j.jphotochem.2003.12.027

[40] Khan, M., et al., Ceramics International, 2020. 46(10): p. 16813-16819; https://doi.org/10.1016/j.ceramint.2020.03.256

[41] Tian, H., et al., Journal of Physical Chemistry C, 2010. 114(3): p. 1627-1632; https://doi.org/10.1021/jp9103646